Catalysis Letters (2018) 148:2472–2479
https://doi.org/10.1007/s10562-018-2469-2

Preparation of TiO_2 Nanotube Supported Pd for the Hydrogenation of 4-carboxy-benzaldehyde

Jingwei Liu[1] · Wenbin Du[1] · Zezhuang Li[1] · Aiwu Yang[1]

Received: 27 April 2018 / Accepted: 19 June 2018 / Published online: 2 July 2018

Abstract

Mesoporous TiO_2 nanotube (TNT) with high surface area was synthesized and used to support palladium. The as prepared Pd/TNT was characterized by different physico-chemical techniques, such as XRD, SEM, TEM, N_2 physisorption, CO chemisorption and XPS. The catalytic behavior for the hydrogenation of 4-carboxy-benzaldehyde was evaluated and compared with that of a commercial Pd/C. It was observed that Pd species was highly dispersed on TNT at a nominal 0.5% loading, and mainly existed in a metallic state. In comparison with this commercial Pd/C, the Pd/TNT displayed a better catalytic performance for the conversion of 4-carboxy-benzaldehyde. At 0.6 MPa and 280 °C, the Pd/TNT tended to catalytically convert 4-carboxy-benzaldehyde into more stable benzoic acid via a decarbonylation process.

Graphical Abstract

A Pd/TNT with high palladium dispersion was successfully prepared by the wet incipient impregnation using a high surface area TiO_2 nanotube support, and the fresh catalyst tended to catalytically convert 4-carboxy-benzaldehyde into more stable benzoic acid in the initial operation stage.

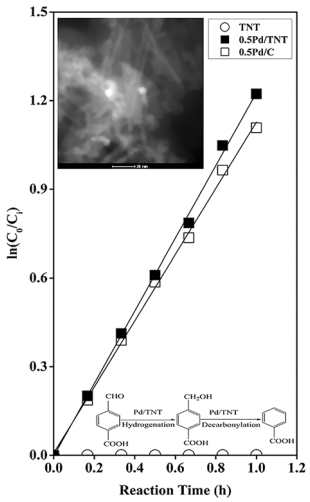

Keywords Mesoporous TiO_2 nanotube · Pd/TNT · Dispersion · Hydrogenation of 4-carboxy-benzaldehyde · Benzoic acid

1 Introduction

One dimensional nanostructured material is one of the most promising supports for redox and acid/base reactions, owing to their unique physical and chemical properties unlike to their bulk counterparts. Among them, titanium oxide

✉ Jingwei Liu
jingweiliu@163.com

[1] Research Institute, Sinopec Yangzi Petrochemical Co., Ltd., Nanjing 210048, China

nanotube (TNT) has high surface area, open mesoporous channel, semiconductor bands gaps and strong electronic synergetic interaction with active sites. Based on these above merits, TNT can support and disperse rather large amounts of active species, and also facilitate fast transportation of reagents and products. Hence, TNT has found wide application in many catalytic processes, including selective catalytic reduction of ammonia [1, 2], oxidation of carbon monoxide [3, 4] and dibenzothiophene [5, 6], selective catalytic oxidation of alcohols [7–10], double-bond migration [11], water–gas shift reaction [12], hydroformylation [13, 14], hydrodesulphurization [15] and alkylation [16].

Terephthalic acid (TA) is a core aromatic starting material to polyester fibers manufacture development, and mostly produced by liquid phase aerobic oxidation of p-xylene in the acetic acid medium using $Co(OAc)_2$ and $Mn(OAc)_2$ homogeneous catalysts with a bromine promoter, as described in a process commonly known as the BP-AMOCO technology. In the oxidation process, some intermediate oxidation impurities such as 4-carboxy-benzaldehyde (4-CBA) and several colorful polyaromatics are accompanied by terephthalic acid (TA). In order to obtain purified terephthalic acid conforming to polymerization grade standard, crude terephthalic acid must be dissolved in hot water at 270–280 °C, and followed by hydrogenation in a trickle bed reactor, where activated carbon supported palladium species are demonstrated as an excellent catalyst with good resistance to hot acid corrosion. In pursuit of satisfactory catalytic performance of carbon based catalysts, Menegazzo et al. observed that the Pd/C possessed high metal dispersion and good reactivity at the pH of the impregnating palladium precursor solution ranging from 1.5 to 2 [17]. Jhung et al. [18] incorporated inexpensive ruthenium into Pd/C to prevent the sintering of Pd, and the bimetallic catalyst displayed a higher activity and stability than the single Pd catalyst. Zhu et al. [19] investigated the effect on hydrogenation process on product distribution over a monolith based carbon fiber supported Pd, and emphasized to present a consecutive reaction mechanism, namely an intermediate product 4-hydroxymethyl benzoic acid (4-HMBA) and another deep hydrogenation product p-toluic acid (PA). Similar reaction characteristic was also previously observed by Li et al. [20].Although mentioned above, the activated carbon supported catalysts still suffer from drawbacks such as low crush strength and abrasion resistance, leading to the palladium leaching and contamination of downstream products. In order to avoid without the loss in reactivity, one support comprising titanium oxide have been developed as an excellent substitute for carbon supports in the past decades. For example, preparation of titanium dioxide supported one and more metals belonging to group VIII for the efficient removal of 4-CBA was disclosed in patents, which were assigned to Amoco and Degussa [21–23], respectively. Besides the single TiO_2 support, Zhou et al. [24] found that titanium incorporated Pd/CDC–SiC was significantly more active than unmodified Pd/CDC–SiC toward the hydrogenation of 4-carboxybenzaldehyde, due to the increasing dispersion of Pd.

It is well known that a carrier with higher surface area is beneficial for the dispersion of active sites, and further improve catalytic reactivity. Inspired by the fact that conventional titanium dioxide is a suitable support for the hydrogenation of 4-CBA, we thought that TNT supported palladium should display superior catalytic performance. Herein, we report an effective and cost saving synthetic strategy of TNT supported palladium materials, and the synthesized Pd/TNT were characterized by N_2 adsorption, X-ray diffraction (XRD), X-ray photoelectron microscopy (XPS), inductively coupled plasma spectrometry (ICP), scanning electron microscopy (SEM) and transmission electron microscopy (TEM), CO chemisorption. Furthermore, their catalytic activity are evaluated by means of hydrogenation of 4-CBA, and a wide product distribution including 4-hydroxymethyl benzoic acid (4-HMBA), terephthalic acid (TA), p-toluic acid (PA) as well as benzoic acid (BA) is also studied at different catalyst loadings.

2 Experimental Section

2.1 Catalysts Preparation

TNT support was fabricated according to our previous work as reported elsewhere [9]. In a typical procedure, 0.9 g TiO_2 (Degussa P25) was dispersed in 30 ml of 10 M NaOH solution under vigorous stirring for 30 min. After then, the mixture was transferred into a Teflon-lined stainless steel autoclave and maintained at 130 °C in an oven for 24 h. The as-synthesized paste was washed by 0.1 M HNO_3 and 0.05 M HNO_3 in a sequence. Subsequently, it was further washed to neutral by distilled water at 45 °C. Finally, the white paste obtained was dried at 40 °C overnight and then calcined at 400 °C for 1 h.

A Pd/TNT catalyst with a nominal loading of 0.5 weight percentage palladium was prepared by the wetness incipient impregnation. Firstly, TNT was added into the aqueous solution containing an appropriate amount $PdCl_2$ at pH of 2, and the slurry was dried at room temperature. Secondly, a desired amount of n-butanol was added into the solid from the first step, and then the second slurry was dried at 80 °C and subjected to annealing at 220 °C for 1 h. Prior to the catalytic test, Pd/TNT was reduced by H_2 at 220 °C for 1 h in order to obtain a high metal dispersion catalyst. The corresponding reduction samples were denoted as 0.5Pd/TNT, where 0.5 refers to the approximate palladium weight percentage in the sample.

2.2 Characterization

Powder X-ray diffraction (XRD) patterns were collected on Shimadzu XRD-6000 diffractometer using Ni-filtered Cu Kα radiation (λ = 0.15418 nm), operated at 40 kV and 30 mA at a scanning rate of 10°/min. The loading of palladium in Pd/TNT was determined by inductively coupled plasma analysis using a PerkinElmer Optima 2100DV.

The surface area, pore sized distribution and pore volume were determined from nitrogen adsorption–desorption analysis at − 196 °C using a Micromeritics ASAP 2020HD analyzer. Prior to the nitrogen sorption, the sample was degassed to 10^{-3} Torr at 200 °C. Scanning electron microscopy images were obtained using a Hitachi S-4800 scanning electron microscope. Transmission electron microscopy (TEM) was performed on a FEI Tecnai G2 F30 S-TWIN microscope with a STEM HAADF detector under an accelerating voltage of 200 kV. The samples were dispersed in acetone under ultrasonic conditions and deposited onto copper grids coated with ultrathin carbon films. X-ray photoelectron spectra (XPS) measurement was performed on a PHI Quantera instrument equipped with a hemispherical electron analyzer and an Al anode (Al Kα = 1486.6 eV). The residual pressure in the spectrometer chamber during data acquisition was 5×10^{-8} Pa. A value of 284.6 eV for the binding energy of the main C1s component was used as an internal calibration standard.

The dispersion of palladium was determined by CO chemisorption at 40 °C after reduction in hydrogen at 220 °C, on a Micromeritics ASAP 2020HD analyzer. Considering the effect of physical adsorption, a similar experimental pathway was carried out in a sequence of first adsorption-evacuation-second adsorption according to previous work. Briefly, the first and second uptake was obtained, and the actual uptake for the sample was calculated by subtracting the second uptake from the first uptake. The dispersion of Pd can be calculated by assuming an adsorption stoichiometry of one CO molecular per surface palladium atom [25]. The mean Pd crystallite size can also be calculated accordingly using a sphere model. For a comparison, a commercial 0.5Pd/C catalyst was used to determine the dispersion in the same manner, where 0.5 was labeled as the approximate palladium weight percentage, and the actual loading determined by inductively coupled plasma was 0.496%.

2.3 Catalytic Test

The reaction of hydrogenation of 4-CBA was carried out in a 100 ml Premex stirred autoclave reactor. In a typical run, 0.2 g or 0.1 g catalyst, 0.7 g 4-CBA and 70 ml deionized water were loaded and reacted at 0.6 MPa and 280 °C. In order to eliminate diffusion effect as soon as possible, the as-prepared Pd/TNT and commercial Pd/C were crushed into 300–400 mesh powder, and the agitation speed maintained at 800 rpm, according to our previous experiment for Pd/C catalyst. Upon termination at some intervals, the reactant and products were determined by an Agilent 1100 Series HPLC equipped with a Hypersil ODS C18 column using acetonitrile-methanol-water ternary mixture as gradient elution mobile phase. The conversion of 4-CBA (T) with selectivity to products (S) was expressed in the following formula:

$$T = \frac{C_0 - C_i}{C_0} \times 100\%$$

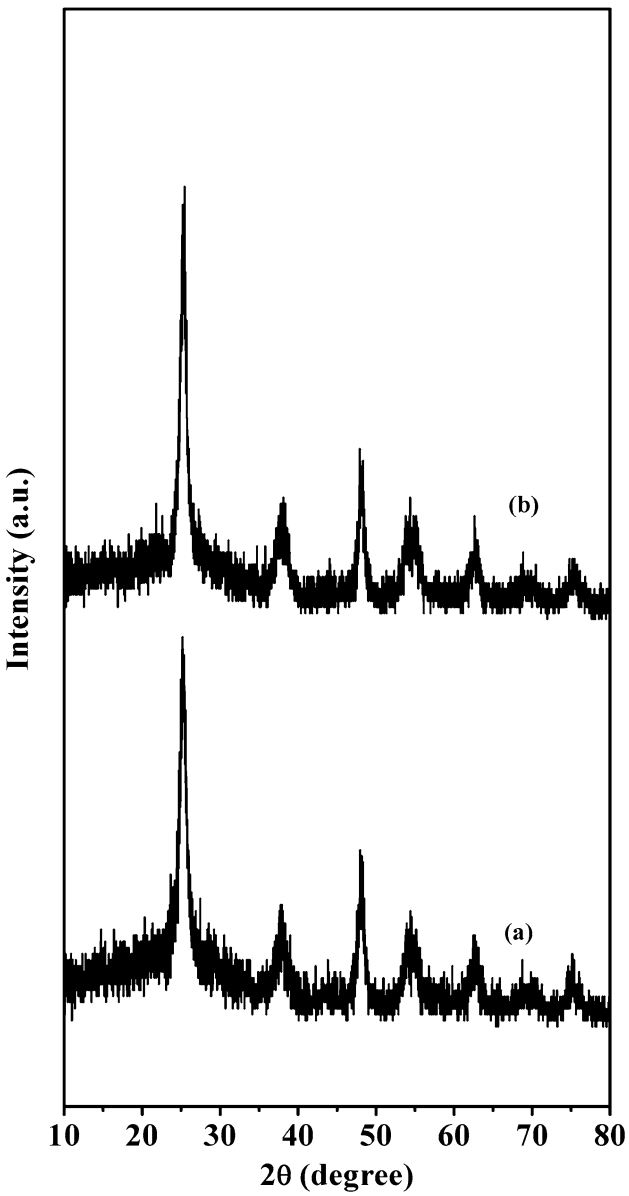

Fig. 1 XRD patterns of TNT (*a*) and 0.5Pd/TNT (*b*)

$$S_{HMBA} = \frac{C_{HMBA}}{C_0 - C_i} \times 100\%$$

$$S_{TA} = \frac{C_{TA}}{C_0 - C_i} \times 100\%$$

$$S_{BA} = \frac{C_{BA}}{C_0 - C_i} \times 100\%$$

$$S_{PA} = \frac{C_{PA}}{C_0 - C_i} \times 100\%$$

where, Ci, C_{HMBA}, C_{TA}, C_{BA} and C_{PA} are represented as the instantaneous molar concentration of 4-CBA, 4-HMBA, BA and PA, respectively. C_0 is the initial molar concentration of 4-CBA.

3 Results and Discussion

Figure 1 shows the XRD patterns of the TNT and the 0.5Pd/TNT. Five main characteristic peaks at 25.3°, 37.8°, 48.1°, 55.2° and 68.6° assigned to anatase (JCPDS references 21-1272) are observed on the TNT, in accordance with our previous result [9]. After loading of palladium followed by reduction in hydrogen, the intensity of anatase reflection peaks did not seem to change, and also no signals corresponding to palladium species were noticeable, indicating the high dispersion of palladium species on the TNT at such a low Pd amount. Hanaor and Sorrell [26] reviewed the incorporation of Pd into TiO_2 brought about the phase transformation from anatase to rutile. However, this phenomenon was not occurred for the 0.5Pd/TNT, owing to low Pd amount and low reduction temperature. Inductively coupled plasma analysis showed that the actual weight percentage of Pd in the 0.5Pd/TNT is 0.482, lower than the nominal palladium composition. Accordingly, it was calculated that the atomic ratio of Ti to Pd is 275.

For the TNT, SEM image in Fig. 2a shows the presence of messy bundles comprising many tiny rod-like filaments, and the length ranged from tens to hundreds of nanometers. After loading of Pd, the rod-like structure was still well preserved in Fig. 2b. For the TNT and its counterpart supported catalyst, the tubular structure with 100–200 nm in length and 10–15 nm in outside tubular diameter was further verified from TEM investigation in Fig. 2c, d. HAADF STEM

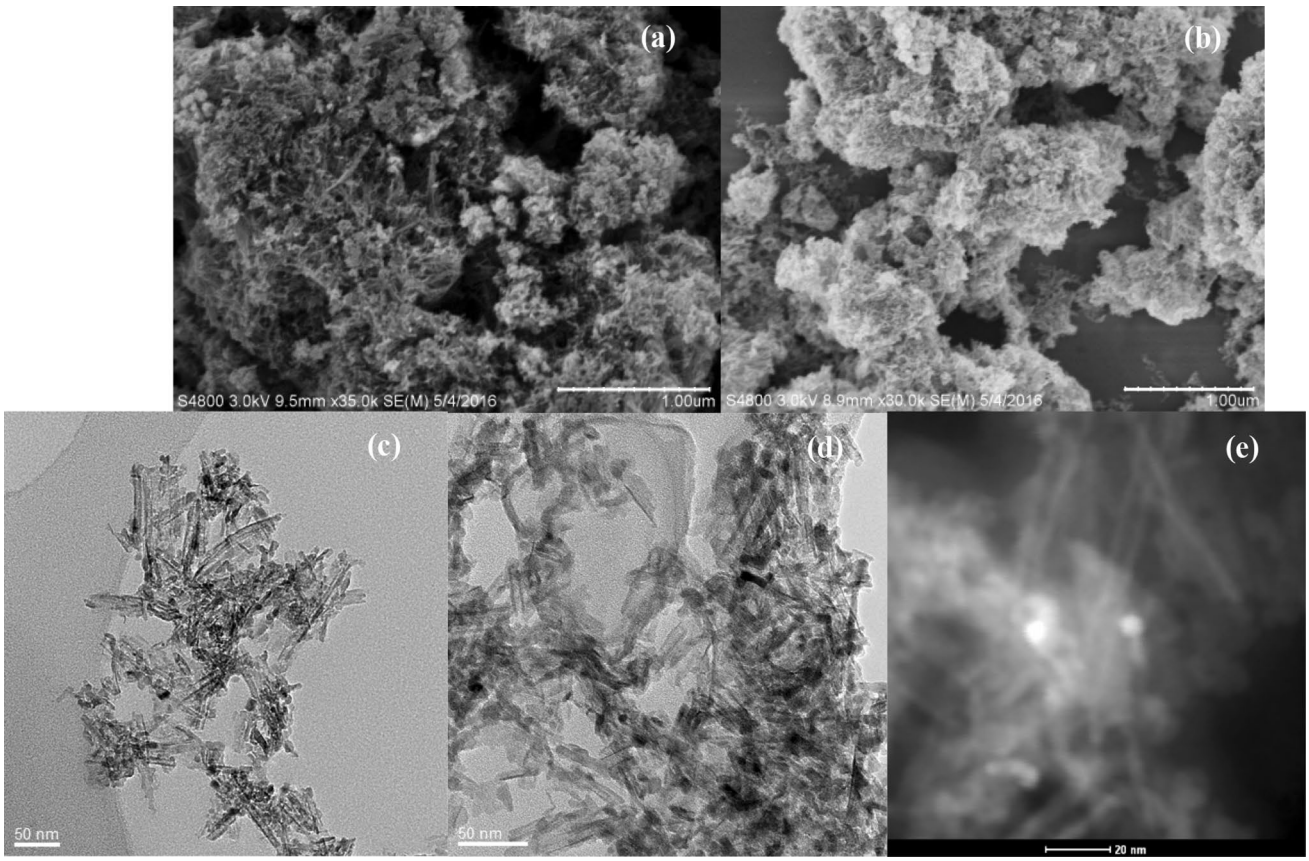

Fig. 2 **a** Overview TNT SEM micrograph, and **b** overview 0.5Pd/TNT SEM micrograph, and **c** TNT TEM image, and **d** 0.5Pd/TNT TEM image, and **e** HAADF STEM of 0.5Pd/TNT

analysis (Fig. 2e) indicated the presence of highly dispersion of Pd and the crystallite diameter between 1 and 4 nm.

Figure 3 gives the nitrogen adsorption–desorption isotherms and corresponding BJH pore size distributions from desorption branch for the TNT and 0.5Pd/TNT samples, and their textural parameters are listed in Table 1. For these two samples, typical IV isotherms with a H3 hysteresis loop can be observed, indicative of slit-shaped mesoporous structure. As shown in Table 1, the TNT possesses a high surface area of 307 $m^2\ g^{-1}$ with an average pore width of 13.6 nm. Comparatively, the 0.5Pd/TNT has a rather lower surface area of

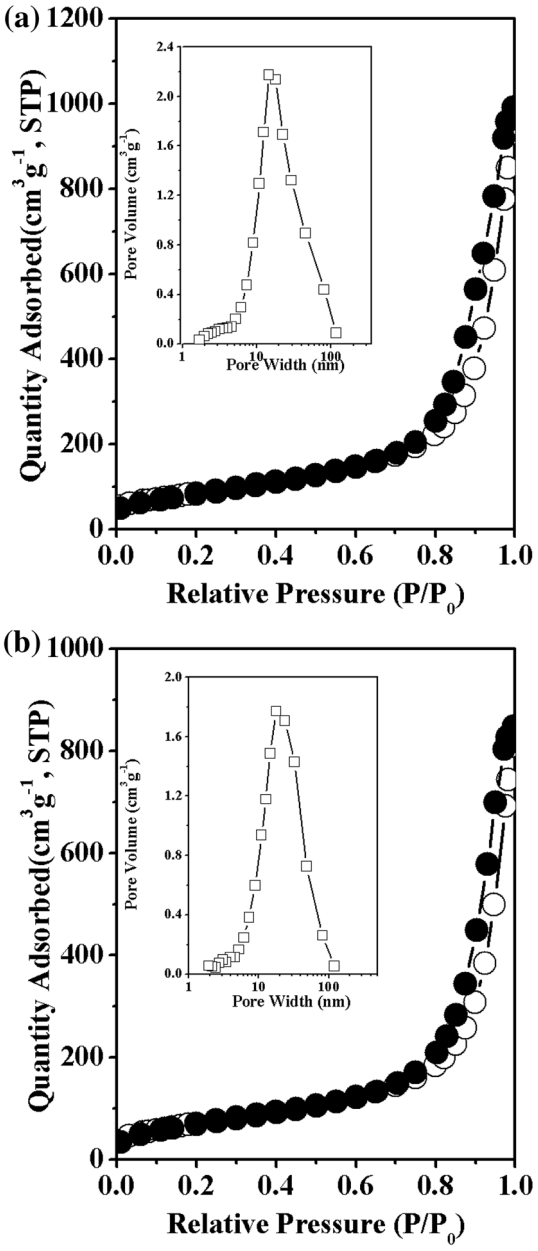

Fig. 3 N_2 adsorption–desorption isotherms and pore size distribution from the desorption branches for TNT (**a**) and 0.5Pd/TNT (**b**)

260 $m^2\ g^{-1}$ with 1.31 $cm^3\ g^{-1}$ pore volume, which can be attributed to the blocking or the partial collapse of nanotubular pore size due to palladium crystallite size. The difference in tubular diameter determined from TEM investigation and pore size from nitrogen adsorption was noticed, since the latter adsorption method gave an average pore size including nanotubular and nanotubular packing porosity.

The chemisorption of CO has been used to determine the dispersion of noble metal on supports. Due to the fact of strong metal support interaction and sintering agglomeration, the actual number of accessible active sites is lower than its theoretical value, where the ratio is usually defined as metal dispersion. In order to avoid the weakly reversible adsorption, i.e. physical adsorption, the obtained difference between first isotherm and second isotherm should be an accurate amount reflecting real chemical adsorption, as described in many previous works [27–30]. As seen in Table 1 calculated from Fig. 4, the dispersion for the 0.5Pd/TNT was 42.8%, and the mean Pd crystallite diameter based on the spherical model was 2.67 nm, in accordance with the TEM investigation. Therefore, it was reasonable that such small palladium crystallite on TNT could not be detected by the XRD technique. The 0.5 Pd/C catalyst used as a reference possessed a slightly lower dispersion of 40.2% with a crystallite diameter of 2.78 nm.

XPS was applied to measure the composition and chemical state of all elements on the surface of 0.5Pd/TNT. Table 2 gives the data about the surface composition for the 0.5Pd/TNT. The surface atomic ratio of Ti to Pd is 256, which is slightly lower than the global ratio of Ti to Pd, suggesting that the Pd species on the surface of TNT were enriched. As shown in Fig. 5, XPS spectra due to the Pd $3d_{5/2}$ orbital was deconvoluted into two fitting peaks at ca. 335.0 and 336.9 eV, attributable to the binding energy of metallic Pd and oxidative Pd or Pd species bearing a strong metal-support interaction [31], respectively. The inspection result revealed that the metallic Pd was predominant over other oxidative states among these Pd species. Considering that 0.5Pd/TNT was primarily reduced in hydrogen for 2 h prior to the XPS analysis,it was as expected that most of Pd species might be in its metallic state.

According to previous works, hydrogenation of 4-CBA was usually regarded to follow the first order kinetics [17, 24]. Thus, the Napierian logarithm of the initial concentration of 4-CBA (C_0) divided by the instantaneous concentration (C_i) at a given time is a liner relationship with reaction time, assuming that the apparent reaction rate constant is invariable during the reaction period. Figure 6 displays the results of hydrogenation of 4-CBA over the TNT, 0.5Pd/TNT and 0.5Pd/C with time on stream at a catalyst loading of 0.2 g. The TNT exhibited a very poor reactivity for the hydrogenation of 4-CBA and the conversion is almost below 0.5%. In contrast, the conversion of 4-CBA was dramatically

Table 1 Surface areas, pore parameters, dispersion and metal particle size

Sample	S_{BET} ($m^2\ g^{-1}$)	Pore size (nm)	Pore vol. ($cm^3\ g^{-1}$)	Dispersion (%)	Pd crystallite size (nm)
TNT	307	13.6	1.53	–[a]	–[a]
0.5Pd/TNT	260	16.6	1.31	42.8	2.62
0.5Pd/C	851	2.7	0.45	40.2	2.78

[a]Not available

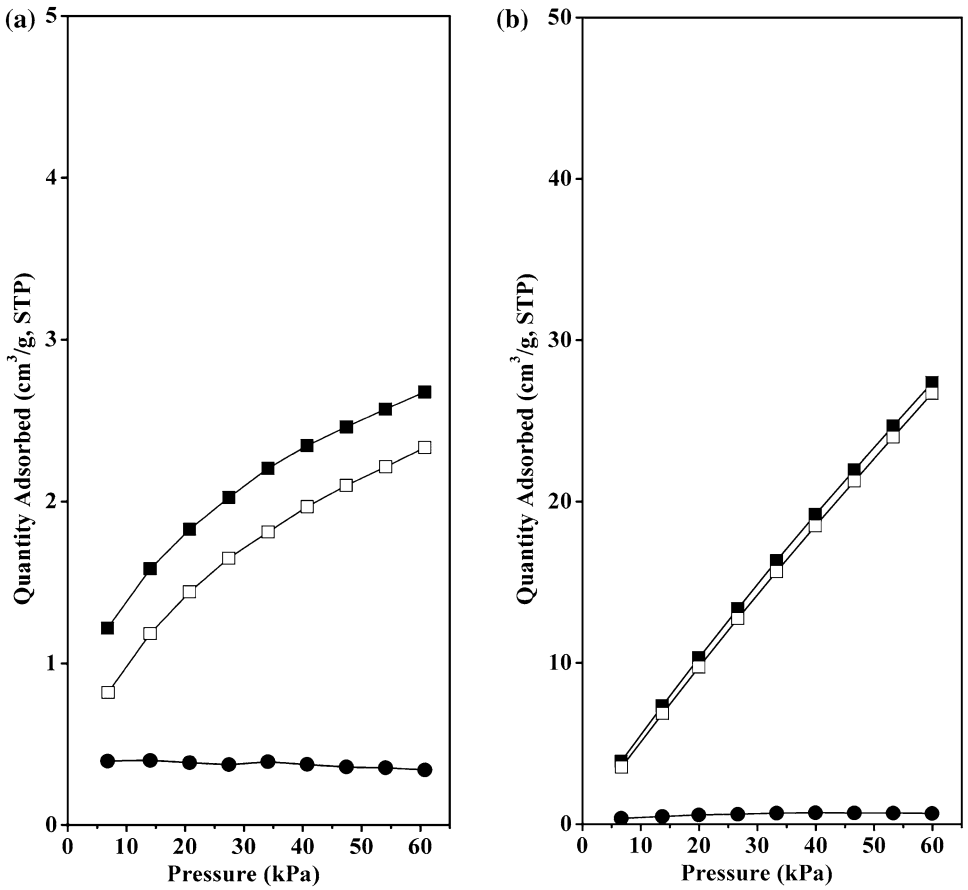

Fig. 4 CO chemisorption for 0.5Pd/TNT (**a**) and 0.5Pd/C (**b**): ■ first adsorption, □ second adsorption, ● difference adsorption

Table 2 Binding energies at Pd 3d orbital level and surface composition

Sample	$Pd3d_{5/2}$ fitting peak location (eV)		Surface composition (%)			
	Metallic state	Oxidative state	Pd	O	Ti	C
0.5Pd/TNT	335.0	336.9	0.1	47.9	25.6	26.4

enhanced over the 0.5Pd/TNT, due to the high dispersion of Pd active sites. In spite of the relatively higher surface area, the 0.5Pd/C was less active than the 0.5Pd/TNT, which might be connected with the poor dispersion and large crystalline dimension. The corresponding apparent reaction rate constants for TNT and 0.5Pd/TNT as well as 0.5Pd/C were 1.9×10^{-4}, 1.23 and 1.12 h^{-1}, respectively.

Table 3 gives the product distribution of 4-CBA hydrogenation over the 0.5Pd/TNT after an hour under similar condition, except for the different catalyst loading of 0.1 and 0.2 g. Earlier most studies reported that hydrogenation of 4-CBA proceed in two consecutive steps to p-toluic acid (PA) as a main goal product via 4-hydroxymethyl benzoic acid (4-HMBA) as a main intermediate product [19, 20]. However, it is not the case in the present work and our initial

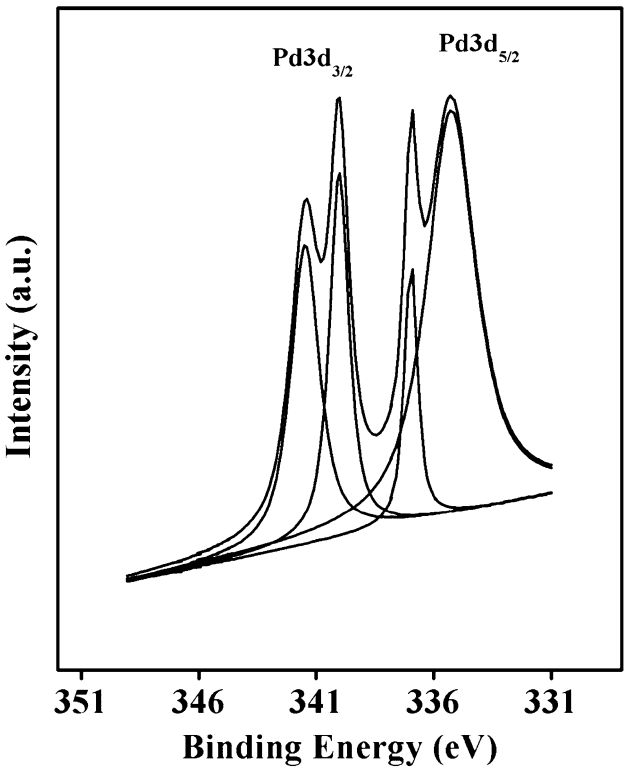

Fig. 5 XPS spectra of Pd 3d core level of 0.5Pd/TNT

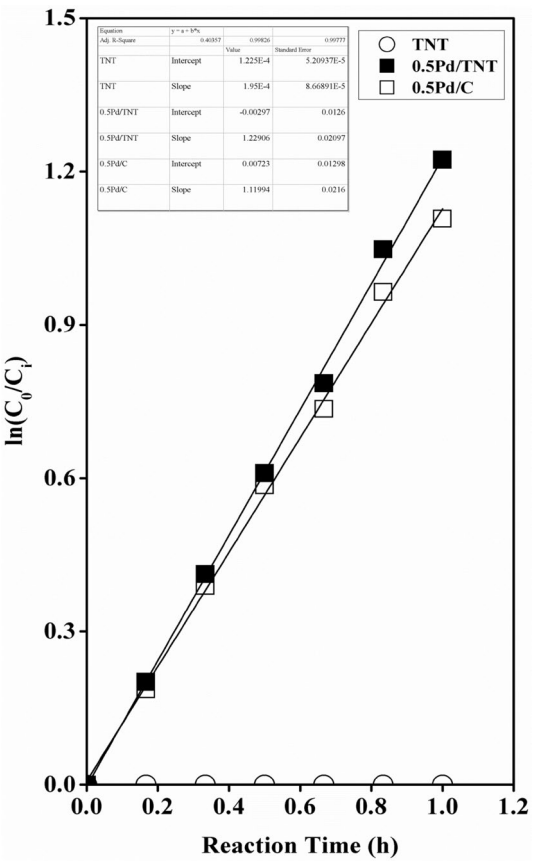

Fig. 6 Hydrogenation of 4-CBA over TNT, 0.5Pd/TNT and 0.5Pd/C with time on stream in the case of 0.2 g catalyst loading

operation stage of PTA industry plant, due to high catalytic reactivity and trace amount of oxygen [32]. It is worth noting that the 0.5Pd/TNT exhibited good decarbonylation performance for the formation of benzoic acid studied in this work. For example, in the case of 0.1 g catalyst loading, the main product is 4-HMBA with 55.1% selectivity, while selectivity to PA is only 4.8%. When the catalyst amount increased to 0.2 g,most of 4-HMBA and PA was further decarbonylated to benzoic acid, and the selectivity to benzoic acid reached as high as 82.0 with 96.8% 4-CBA conversion. Comparatively, conversion of 4-CBA over the commercial 0.5Pd/C was 91.1 with 75.9% selectivity to BA. When the 4-CBA conversion reached about 96% over the 0.5Pd/C by prolonging reaction time, the selectivity to PA and BA were 15.4 and 70.3%, while the selectivity to TA and 4-HBA decreased to 1.7 and 12.6%. According to the accessible Pd amount calculated in Table 1 and conversion of 4-CBA in Table 3, TOF (turn over frequency) for 0.5Pd/TNT and 0.5Pd/C was 1125 and 1127 h^{-1}, respectively. Although TOF for 0.5Pd/TNT was slightly lower than it for 0.5Pd/TNT, 0.5Pd/TNT exhibited comparatively better hydrogenation conversion of 4-CBA due to more accessible Pd number, further verifying the positive effect of good dispersion and small crystalline size.

Table 3 Product distribution of 4-CBA hydrogenation over the 0.5Pd/TNT catalyst with different loading, and a commercial 0.5Pd/C for comparison at the same condition

Catalyst and loading (g)	Conv. (%)	Selectivity (%)			
		4-HMBA	TA	BA	PA
0.5Pd/TNT, 0.2	96.8	13.4	3.7	82.0	0.9
0.5Pd/TNT, 0.1	74.3	55.1	14.9	25.2	4.8
0.5Pd/C, 0.2	91.1	14.8	2.5	75.9	6.8

4 Conclusions

Herein, a 0.5Pd/TNT was successfully prepared by the wet incipient impregnation using a high surface area TiO_2 nanotube support. It is evidenced that Pd species with 1–4 nm crystallite size was highly dispersed and more enriched on the surface of TNT. In terms of hydrogenation of 4-CBA, the 0.5Pd/TNT exhibited superior catalytic performance than the 0.5Pd/C, and the corresponding apparent reaction rate constants were 1.23 and 1.12 h^{-1}, respectively. Over this 0.5Pd/TNT, the 4-CBA was preferentially hydrogenated to

an immediate 4-HMBA molecule, and subsequently decarbonylate to form a more stable benzoic acid molecule with increasing catalyst loading.

Acknowledgements We thank Dr. Yanwen Ma for help with SEM investigations at Nanjing University of Posts and Telecommunications. Financial support from Science and technology support project of Jiangsu Province (BE2013101) is gratefully acknowledged.

Compliance with Ethical Standards

Conflict of interest The authors declare that they have no conflict of interest.

References

1. Mejía-Centeno I, Castillo S, Camposeco R et al (2015) Chem Eng J 264:873
2. Nian JN, Chen SA, Tsai CC et al (2006) J Phy Chem B 110:25817
3. Zhang P, Guo JL, Zhao P et al (2015) RSC Adv 5:11989
4. Zhu BL, Zhang XX, Wang SR et al (2007) Microporous Mesoporous Mater 102:333
5. Cortes-Jácome MA, Morales M, Angeles Chavez C et al (2007) Chem Mater 19:6605
6. Lorencon E, Alves DCB, Krambrock K et al (2014) Fuel 132:53
7. Herrera JE, Isimjan TT, Abdullahi I et al (2012) Appl Catal A 417:13
8. Nepak D, Darbha S (2015) Catal Commun 58:149
9. Liu JW, Fu YC, Sun Q et al (2008) Microporous Mesoporous Mater 116:614
10. Bavykin DV, Lapkin AA, Plucinski PK et al (2005) J Catal 235:10
11. Torrente-Murciano L, Lapkin AA, Bavykin DV et al (2007) J Catal 245:272
12. Sato Y, Koizumi M, Miyao T et al (2006) Catal Today 111:164
13. Hu XJ, Shi YK, Zhang YJ et al (2015) Catal Commun 59:45
14. Shi YK, Hu XJ, Zhu BL et al (2014) RSC Adv 4:62215
15. Palcheva R, Dimitrov L, Tyuliev G et al (2013) Appl Surf Sci 265:309
16. Li SS, Li N, Li GY et al (2015) Appl Catal B 170:124
17. Menegazzo F, Fantinel T, Signoretto M et al (2007) Catal Commun 8:876
18. Jhung SH, Romanenko AV, Lee KH et al (2002) Appl Catal A 225:131
19. Zhu J, Wu F, Li M et al (2015) Appl Catal A 498:222
20. Li KT, Hsu MH, Wang K (2008) Catal Commun 9:2257
21. Rosen BI, Bartos TM (1997) US 5756833
22. Schroeder H, Wittman RL (1994) WO 9420447
23. Bankmann M, Brand R, Freund A et al (1994) US 5387726
24. Zhou YH, Li XY, Pan XL et al (2012) J Mater Chem 22:14155
25. Groppo E, Agostini G, Piovano A et al (2012) J Catal 287:44
26. Hanaor DAH, Sorrell CC (2011) J Mater Sci 46:855
27. d'Alnoncourt RN, Friedrich M, Kunkes E et al (2014) J Catal 317:220
28. Srebowata A, Tarach K, Girman V et al (2016) Appl Catal B 181:550
29. Santiago M, Restuccia A, Gramm F et al (2011) Microporous Mesoporous Mater 146:76
30. Neal LM, Everett ML, Hoflund GB et al (2011) J Mol Catal A 335:210
31. Kast P, Friedrich M, Teschner D et al (2015) Appl Catal A 502:8
32. Azarpour A, Zahedi G (2012) Chem Eng J 209:180